Indian Journal of Pure & Applied Physics
Vol. 53, July 2015, pp. 447-455

Investigation of gain characteristics of GRIN-InGaAsP/InP nano-heterostructure

Rashmi Yadav[1], Meha Sharma[2], Swati Jha[2], Pyare Lal[1], M J Siddiqui[3], F Rahman[4], S Dalela[5] & P A Alvi[1]*

[1]Department of Physics, Banasthali Vidyapith, Rajasthan 304 022, India

[2]Department of Electronics, Banasthali Vidyapith, Rajasthan 304 022, India

[3]Department of Electronics, Z. H. College of Engineering & Technology, Aligarh Muslim University, Aligarh 202 002 (UP), India

[4]Department of Physics, Aligarh Muslim University, Aligarh 202 002 (UP), India

[5]Department of Pure & Applied Physics, University of Kota, Kota, Rajasthan, India

*E-mail: drpaalvi@gmail.com

Received 11 December 2014; revised 31 March 2015; accepted 15 May 2015

The modal gain characteristics along with optical losses theoretically within TE and TM polarization modes for GRIN-$In_{0.90}Ga_{0.10}As_{0.59}P_{0.41}$/InP lasing nano-heterostructure by taking into account the number of quantum wells as active layers inserted between barriers, have been investigated in the present paper. In addition, the behaviour of saturated modal gain, transparency current density and maximum optical loss for the single and multiple quantum wells based nano-heterostructures, has also been studied. Moreover, temperature and GRIN dependence of modal gain characteristics with in TE and TM mode have been studied. Under simulation, the anti-guiding factors (a substantial parameter for optical gain) along with modal gain as a function of photonic energy and lasing wavelength at different temperatures have also been investigated. The maximum gain is achieved in the NIR (near infrared) regions at the wavelengths ~1.40 μm and ~1.25 μm in TE and TM polarization modes, respectively in the present paper. Hence, the nano-structure studied in this work is very useful as a light source for the optical fiber based communication system functioning in the NIR region due to less attenuation.

Keywords: InGaAsP, Nano-heterostructure, Modal gain, Transparency current density, Anti-guiding factor

1 Introduction

The material InGaAsP/InP system based multiple quantum well (MQW) lasing heterostructures is widely used in optical fiber communication system as light sources due to their interesting lasing wavelengths. Quantum well (QW) lasing nano-heterostructures are important for research due to their physically and technological properties. In past few decades, the III-V compound semiconductors based quantum well structures have been preferred for lasing applications and steadily grown until now. Recently, due to unusual properties of III-V semiconductors based quantum-size structures; they have drawn a very serious attention of researchers. Interestingly, formation of self-organized low-dimension semiconductor layers has drawn attention to the researchers due to the possibility of creating three-dimensional electron confinement in the uniform and coherent (non-dislocation) clusters. In the present era, quantum size-lasing heterostructures are very significant sources for fiber optic communications and are the key components of applications such as optical data storage and remote sensing[1,2]. In quantum well based lasing heterostructures, it is desirable to lower the threshold current before lasing begins, maximize optical gain and minimize the losses. Step index profile based Separate Confinement Heterostructures (SCH) play a promising role in this context. In SCH designs, the carriers get confined by heterostructure barriers so as to increase the carrier density in quantum well and therefore, enhancing radiative recombination. As a result, a considerable amount of carriers is no more able to drift away towards opposite electrode; they must recombine in the active region. The major benefits are continuous wave operation making them ideal for optoelectronic applications. Further, advantages include less heat generation and less power consumption.

However, the GRIN (Graded Index)-quantum structures have been reported with various advantages over STIN-heterostructures such as greater trapping

and injection efficiency and noticeably shorter doping time and enhanced carrier confinement within the active or quantum region[3-6]. The maximum optical gain of the order of 8000/cm, however, has been reported by Alvi *et al*[7]. for GRIN InGaAlAs/InP structures. Wang Yang *et al*[8]. fabricated 1.5 µm InGaAsP/InP tunnel injection multiple quantum well Fabery Perrot (F-P) ridge laser[8], and investigated the cavity length dependence of temperature T_0. InGaAsP quantum well active region generates good electrical confinement and large amount of gain leads to high quantum efficiency and low threshold current density[9]. By using the 4x4 Luttinger-Kohn Hamiltonian, the optical gain and valence band effective masses in both types of QW lasing structures viz. InGaAlAs and InGaAsP under the influence of compressive strain have been calculated[10]. Carsten *et al*[11]. have presented that by varying the composition and changing the well thickness, the band gap of QWs can be engineered which is the major advantage[11]. In a recent research, theoretical model of AlGaN/GaN, AlInN/InN (Refs 1, 2, 12) and InGaN/InN (Ref.13) material based multilayer nano-heterostructures taking strain effects at the heterointerfaces into account have been analyzed and reported. Specifically, the strain effects of InGaN/InN multi quantum well hetero-systems with different indium contents have been studied with the help of HRXRD (High resolution X-ray diffraction) technique[14]. Moreover, the effect of structural parameters on 2DEG (two dimension electron gas) density and *C~V* characteristics of AlGaN/GaN-based HEMT (high electron mobility transistor) have been studied[15]. Also, lasing characteristics such as material gain, differential gain, anti-guiding factor, and gain compression of AlGaAs/GaAs lasing structure have been studied[16]. In addition, the phenomena of photoluminescence (PL) in such heterostructures have been determined by radiative recombination of excitons[17]. The PL and PL delay time are found to depend on temperature. Moreover, double barrier resonant tunneling structures of material combination InGaAs/AlAs based micro-accelerometers have been designed and fabricated successfully by using control hole technique[18].

2 Structure and Theoretical Details

In a practical quantum well laser, separate confinement heterostructure (SCH) is commonly used to achieve the optical confinement and high injection quantum efficiency. In a SCH QW structure, the QW active region is sandwiched between two optical confining layers (OCLs). The OCL thickness is of the order of the optical wavelength of the lasing region. Basically, there are two types of SCH: Step SCH and GRIN SCH. In step SCH, the refractive index of the QW region is uniformly distributed and changes abruptly at the interfacing of well and barrier region; while in GRIN SCH, the index of the QW region is distributed non-uniformly. In the present study, various lasing characteristics of the GRIN SCH type lasing nano-heterostructure have been investigated theoretically. The structure model has multiple quantum wells (MQWs) sandwiched between the barriers followed by the claddings. The overall structure is assumed to be grown on InP substrate. $In_{0.90}Ga_{0.10}As_{0.59}P_{0.41}$ composition has been utilized as an active region (quantum region). The width of the active region is ~ 6 nm, while the barriers and claddings are of width ~ 5 and 10 nm, respectively, thereby creating a nano-heterostructure. The composition of active region is chosen such that its refractive index is higher than that of barriers while the band gap of active region is less than that of barriers. In case of GRIN structure, it is important to note that the refractive indices of the barriers sandwiching the quantum wells (quantum regions) are uniform while the refractive indices of the outer barriers decrease towards cladding gradually. The physical structure of GRIN type lasing nano-heterostructure is shown in Fig. 1. The barriers out of quantum region have been shown by different colours, while the colours of barriers within the quantum region are the same (Fig. 1). The light blue colour of barriers refers to low refractive index while

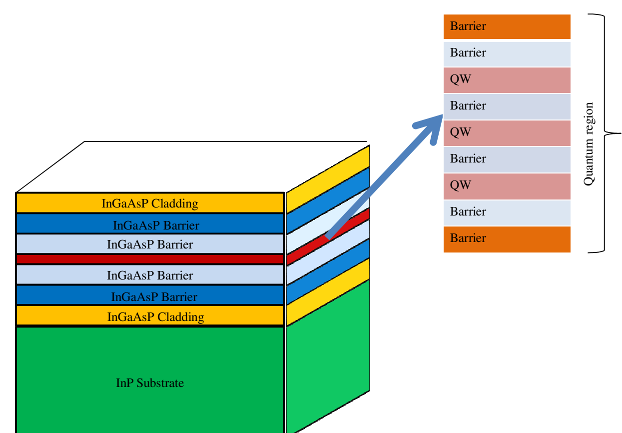

Fig. 1 — Schematic diagram of designed GRIN-InGaAsP/InP Nano-heterostructure

the dark blue indicates high refractive index in the heterostructure.

For evaluation of the discrete energy levels within the semi parabolic conduction band, following equation[19] can be used as:

$$-\frac{\hbar^2}{2m_c^*}\nabla^2\psi + V_c\psi = E_c\psi$$

where ψ is wave function, $\hbar$ the reduced Planck's constant, m_c^* the effective mass of electron in conduction band, V_c the conduction band potential, E_c is electron energy level in conduction band. For a strained quantum well, the conduction band potential is:

$$V_c = \begin{cases} \frac{2\delta_h}{3}, \text{Quantum well} \\ \Delta V_{bc}, \text{Barrier} \\ \Delta V_{cc}, \text{Cladding} \end{cases}$$

where δ_h is the hydrostatic potential and conduction band offsets of barrier and cladding layers are ΔV_{bc} and ΔV_{cc}, respectively. The hydrostatic potential can be defined as:

$$\delta_\hbar = 2a\left(1 - \frac{C_{12}}{C_{11}}\right)\varepsilon$$

where ε is the strain constants of the barrier and quantum well layers that can be given as:

$$\varepsilon = \left(a_b - a_q / a_b\right)$$

where a is the hydrostatic deformation potential, C_{11} and C_{12} are the elastic stiffness constants.

For the purpose of evaluation of wave functions associated with valence sub-bands, the 4×4 Kohn-Luttinger Hamiltonian can be solved as:

$$\hat{H}\psi = \begin{bmatrix} H & M & N & 0 \\ M & L & 0 & N \\ N & 0 & L & -M \\ 0 & N & -M & H \end{bmatrix}\psi = E_v\psi$$

where

$$H = -\frac{\hbar^2}{2m_0}\left[(k_x^2 + k_y^2)(\gamma_1 + \gamma_2) - (\gamma_1 - 2\gamma_2)\frac{\partial^2}{\partial z^2}\right] + V_{hh,lh}$$

$$L = -\frac{\hbar^2}{2m_0}\left[(k_x^2 + k_y^2)(\gamma_1 - \gamma_2) - (\gamma_1 + 2\gamma_2)\frac{\partial^2}{\partial z^2}\right] + V_{hh,lh}$$

$$M = \frac{i\sqrt{3}\hbar^2}{2m_0}(-k_y - ik_y)\gamma_3\frac{\partial}{\partial z}$$

$$N = -\frac{\sqrt{3}\hbar^2}{2m_0}\left[\gamma_2(k_x^2 + k_y^2) - 2i\gamma_3 k_x k_y\right]$$

E_v is the energy Eigen values of valence sub-bands, m_0 is the mass of free electron, γ_1, γ_2 and γ_3 are the Luttinger parameters, k_x and k_y are the components of transverse wave vector, V_{hh}, V_{lh} are the potentials of valence sub-bands for heavy and light holes and can be given as:

$$V_{hh} = \begin{cases} -\frac{1}{3}\delta_h + \delta_s, \text{ Quantum well} \\ -\Delta V_{bv}, \text{ Barrier} \\ -\Delta V_{cv}, \text{Cladding} \end{cases}$$

$$V_{lh} = \begin{cases} -\frac{1}{3}\delta_h - \delta_s, \text{ Quantum well} \\ -\Delta V_{bv}, \text{Barrier} \\ -\Delta V_{cv}, \text{ Cladding} \end{cases}$$

where ΔV_{bv} and ΔV_{cv} are valence band offsets for barriers and claddings, respectively and δ_s is shear potential and it can be expressed as:

$$\delta_s = 2b\left(1 - \frac{2C_{12}}{C_{11}}\right)\varepsilon$$

where b is shear deformation potential.

The optical gain coefficient for quantum well structures[7] can be given as:

$$G(E) = \frac{q^2|M_B|^2}{E\varepsilon_o m_o^2 c\hbar n_{eff} W} \sum_{i,j}\int_{E_g}^{E_{gb}} m_{r,ij} C_{ij} A_{ij}(f_c - f_v) L(E - E^{'}) dE$$

The symbols used have been explained in Refs (7, 16, 19). Where, it may be noted that the L(E) is Lorentzian lineshape function, A_{ij} is angular anisotropy factor and it is normalized in order to have its average as unity. Within TE polarizations, it is given[20] as :

$$A_{ij} = \begin{cases} (3/4)(1+\cos^2\theta), \text{(heavy hole)} \\ (1/4)(5-3\cos^2\theta), \text{(light hole)} \end{cases}$$

For TM polarization, it is given as:

$$A_{ij} = \begin{cases} (3/2)(\sin^2\theta), \text{ (heavy hole)} \\ (1/2)(4-3sin^2\theta), \text{ (light hole)} \end{cases}$$

where the angular parameter is given as:

$$\cos^2\theta = \frac{E'}{E}$$

where E is the photonic energy and E' is the transition energy between i and j states.

The temperature dependence of the optical gain can be expressed as:

$$G(E) = \frac{\pi\hbar e^2}{nEm_0^{\ 2}\varepsilon_0 c}\left[1-\exp(\frac{E-\Delta f}{K_B T})\right] \times \sum_{n_c,n_v} \frac{|M|^2}{4\pi^2 L_W} f_c f_v \frac{\hbar/\tau}{\pi(E_{en}-E)^2+(\hbar/\tau)^2} dK_x dk_y$$

where the symbols used have been explained in Refs (16, 21).

The modal gain (G-J) characteristics of InGaAsP/InP lasing structures can be estimated by the expression as:

$$G_M(J) = \Gamma G(J) = \Gamma G_0(J)\left[\ln\left(\frac{J}{J_0}\right)+1\right]$$

For the MQWs, the above expression will be modified as:

$$n\Gamma G(J) = n\Gamma G_0(J)\left[\ln\left(\frac{J}{J_0}\right)+1\right]$$

where $G_M(J)$ - modal gain, $G(J)$ - material gain and $G_0(J)$ - optimum gain. N is the number of quantum wells in nano-heterostructure. The quantity Γ represents quantum well optical confinement factor, which is defined as:

$$\Gamma = \frac{\int_{-W/2}^{W/2} |\varepsilon(z)|^2 dz}{\int_{-\infty}^{\infty} |\varepsilon(z)|^2 dz}$$

where W is the width of quantum well, $\epsilon(z)$ is the intensity of the electric field of radiation along z-direction.

For multiple quantum wells, the modal gain as a function of transparency current density is given by:

$$n\Gamma G(J) = n\Gamma G_0(J)\left[\ln\left(\frac{nJ}{nJ_{tr}}\right)\right]$$

Threshold current density is calculated as:

$$G_{th}(J) = n\Gamma G(J) = \alpha_i + \frac{1}{2L}\ln\frac{1}{R_1 R_2} = \alpha_i + \alpha_m$$

where α_i and α_m are the internal and mirror loss, respectively. R_1 and R_2 are the mirror reflectivities and L is the cavity length.

Threshold current density in terms of losses can be defined as:

$$J_{th} = \frac{nJ_0}{\eta}\exp\left[\left(\frac{1}{n\Gamma G_0(J)}\right) \times \left(\alpha_i + \frac{1}{2L}\ln\left(\frac{1}{R_1 R_2}\right)-1\right)\right]$$

Next, anti-guiding factor which is a very important parameter has a very crucial role in the heterostructure and it is defined as:

$$\alpha = -\frac{4\pi n'}{\lambda G'}$$

where n' and G' are defined as dn/dN (differential refractive index change) and dG/dN (differential gain), respectively.

3 Results and Discussion

The parabolic nature of dispersion profile of conduction band has been taken into account and 1-D Schrödinger equation has been solved to obtain energy Eigen values of conduction band electrons within the quantum well of the quaternary

semiconductor compound $In_{0.90}Ga_{0.10}As_{0.59}P_{0.41}$ (Fig. 2). The material compositions of quantum wells and barriers are selected in order to have lattice matched criteria, but the selection criteria of the substrate is done in such a way that the quantum wells are compressively strained by an amount of 1.2%, and therefore, for compressively strained structure, proper selection of substrate is very important. In literature, it has been reported that for the compressively strained quantum well structure, TE polarization mode dominates. The compressive conduction and valence bands dispersion profiles for $In_{0.90}Ga_{0.10}As_{0.59}P_{0.41}$ quantum well at temperature 300 K and strain ~ 1.2% are shown in Fig. 2. Apart from the band edge (k_z = 0), the energy of conduction band increases with the propagation vector (or wave vector) and its variation has parabolic nature (Fig. 2). Moreover, the energy separation between conduction band and valence HH (heavy hole) sub-bands increases with increase in wave vector. In addition, according to the valence band dispersion profiles, apart from the band edge, the energy separation between the LH and HH (heavy hole) sub-bands is decreasing but the energy of SO (split off hole) sub-bands with respect to LH and HH valence sub-bands is increasing along the wave vector. The SO hole sub-bands arise due to spin-orbit interactions.

In Figs 3 and 4, the modal gain characteristics of GRIN InGaAsP/InP nano-heterostructure containing SQW and MQWs have been plotted with in both TM and TE polarization modes, respectively, taking into account the effect of number of quantum wells. In general, for the structure with particular number of quantum wells, the modal gain is found to increase with increasing current density and finally fount to saturate at higher current densities. In Figs 3 and 4, it has been predicted that the higher saturated modal gain is achieved with large number of quantum wells at higher current densities. From Figs 3 and 4, the threshold current density and hence, threshold gain can be estimated for a particular number of quantum well in the heterostructure. In both the modes, it is obvious that the threshold current density and threshold modal gain are increased with increasing number of quantum wells in the nano-heterostructure.

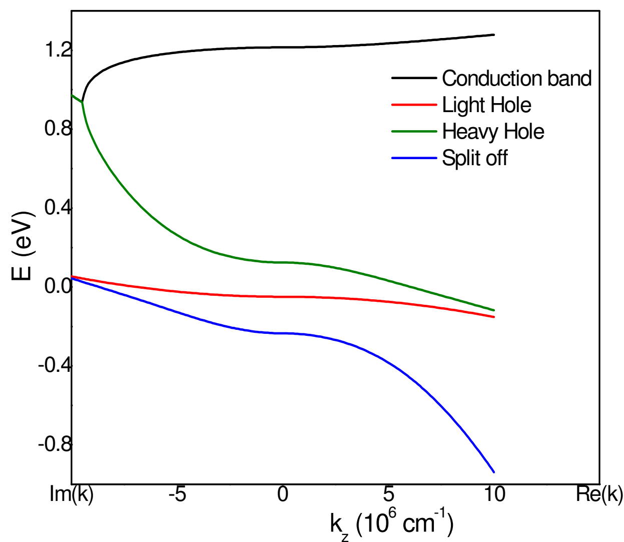

Fig. 2 — Compressive conduction and valence band dispersion profiles for $In_{0.90}Ga_{0.10}As_{0.59}P_{0.41}$ quantum well at 300 K

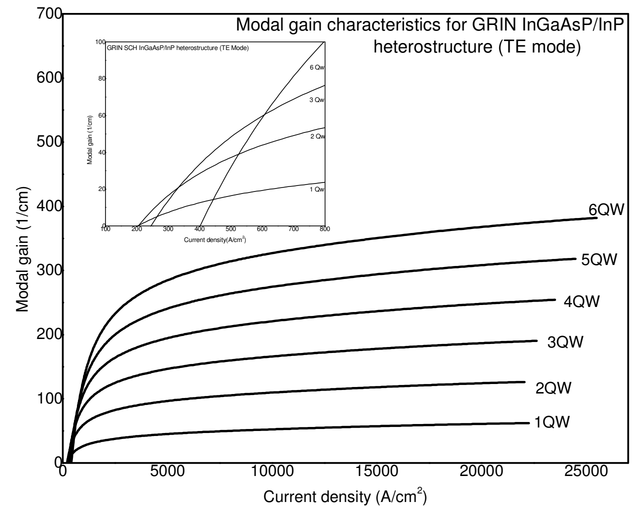

Fig. 3 — Modal gain characteristics for GRIN InGaAsP/InP nano-heterostructures in TE mode

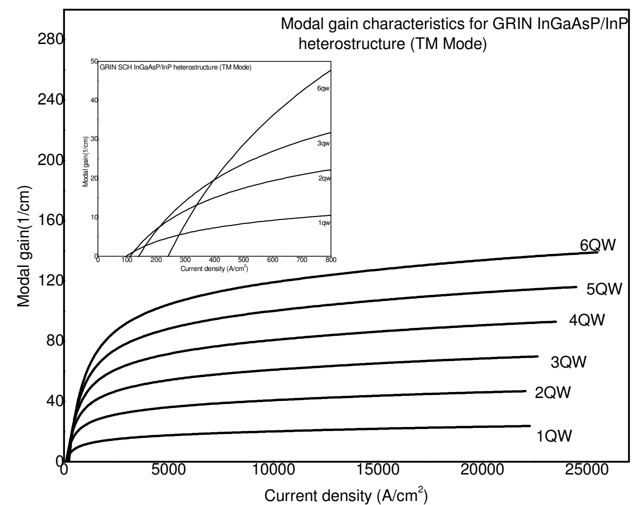

Fig. 4 — Modal gain characteristics for GRIN InGaAsP/InP nano-heterostructures in TM mode

In TE mode, these quantities are greater than that in TM polarization mode; hence TE mode is dominant mode. The similar gain characteristics have been observed for the GRIN structures of InGaAlAs/InP material system[21], but the transparency current density, saturated modal gain and average losses of InGaAsP/InP based heterostructure is found a little greater than that of InGaAlAs/InP based heterostructure.

The TE mode provides higher modal gain in comparison with TM mode, due to the fact that the heavy hole exciton contribution is negligible to the TM polarization mode as compared to the TE mode (Figs 3 and 4). In other words, the momentum matrix element for the heavy hole in the TM mode is almost negligible as compared to that for the heavy hole in the TE mode. Chuang[22] has reported that both TE and TM polarization modes are present in relaxed quantum well structures and these transverse modes broaden the optical spectrum which is not required, but, since, in the present study, the quantum well structure is compressively strained by an amount of 1.2%, hence the TE polarization mode dominates. The inset pictures of Figs 3 and 4 have shown the behaviour of transparency current density, which has played a very crucial role in determining the threshold condition. The transparency current density exists at zero modal gain for the GRIN InGaAsP/InP nano-heterostructure consisting of SQW and MQWs in both TE and TM modes (Figs 3 and 4). The reason of existing transparency current density at zero modal gain is based on the fact that the modal gain on this transparency current density is balanced by background absorption internal optical loss. The inset Figures 3 and 4 also predict that the existence of overall modal gain occurs at the current density (threshold current density) beyond the transparency current density. Moreover, the values of transparency current density are found to increase with increasing number of quantum wells in both the modes.

In Fig. 5, the behaviour of saturated modal gain is predicted for GRIN InGaAsP/InP lasing nano-heterostructure in both TE and TM modes. The modal gain is found to increase linearly with increasing number of quantum wells and the overall modal gain is found more pronounced in TE mode rather than TM mode. Moreover, the variation in transparency current density with number of quantum wells in both modes is shown in Fig. 6. The TE and TM modes based optical losses with current density for the heterostructures have been shown taking into account number of quantum wells (Figs 7 and 8). The maximum optical losses are predicted at the corresponding current density for the heterostructures consisting of various number of quantum wells. Figures 7 and 8 show that for a particular heterostructure having arbitrary MQWs, the maximum optical loss is more in TE mode rather than in TM mode. Though the optical loss for SQW based nano-heterostructure is low, even that the MQWs based structures are preferred because at high loss, the MQWs based nano-heterostructure has the advantage. Its modal gain arises from the part of the modal gain-current density curve that has a high slope rather than

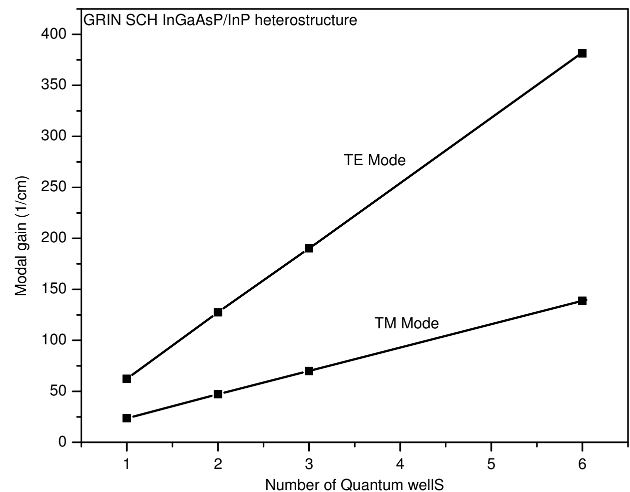

Fig. 5 — Behaviour of saturated modal gain in TE and TM modes

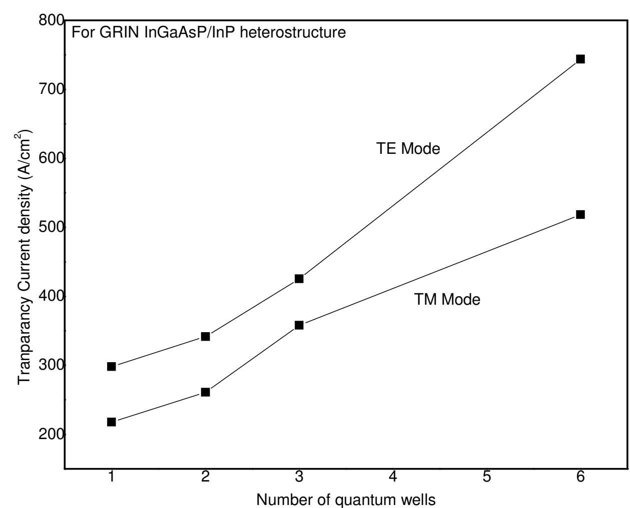

Fig. 6 — Comparison of transparency current density in TE and TM modes

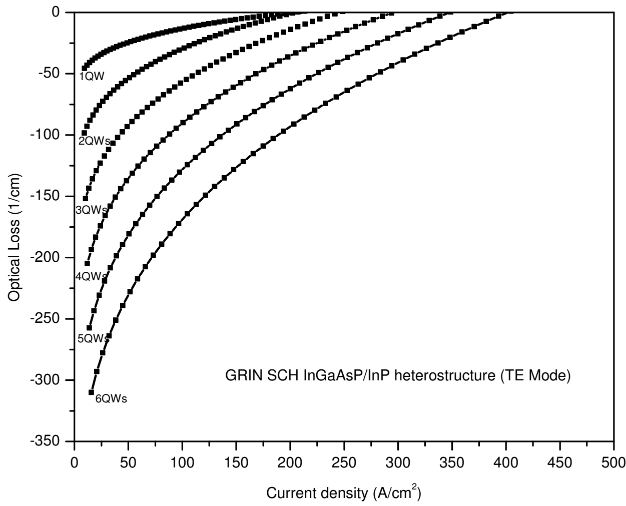

Fig. 7 — Optical losses for GRIN InGaAsP/InP in TE mode

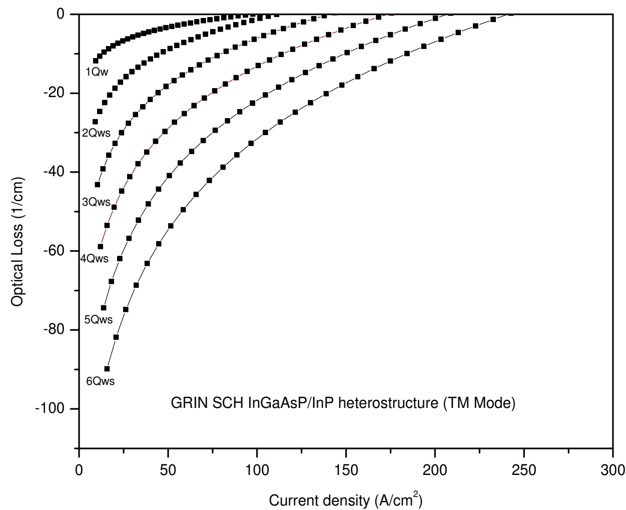

Fig. 8 — Optical losses for GRIN InGaAsP/InP in TM mode

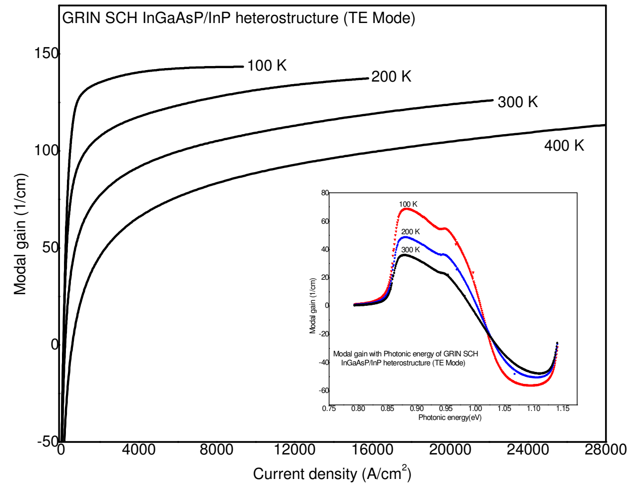

Fig. 9 — Behaviour of temperature dependent modal gain within TE mode

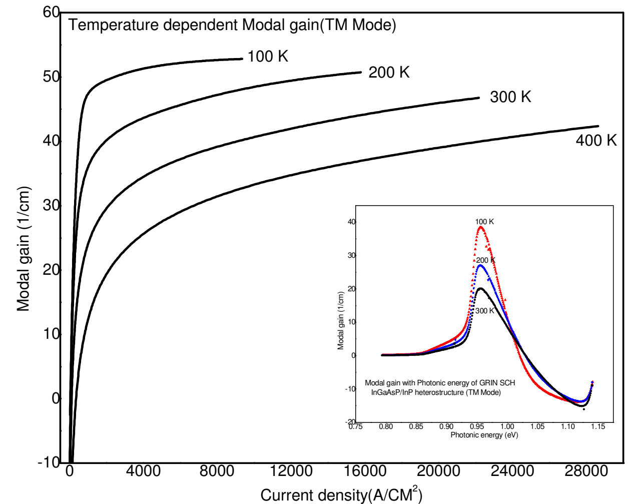

Fig. 10 — Behaviour of temperature dependent modal gain within TM mode

the saturated part as in the SQW lasing nano heterostructure. Since the saturated modal gain of the SQW nano-heterostructure may not be large enough to attain the threshold modal gain and therefore, we must turn to the MQWs lasing nano-heterostructure.

In Figs 9 and 10, the behaviour of temperature dependent modal gain characteristics for the nano-heterostructure consisting of a particular number of quantum well within both TE and TM modes is predicted. The modal characteristics are shifting downwards with increasing temperature, thereby decreasing threshold current densities. This effect is due to more injected carriers elevated to higher state and more holes populated in the GRIN SCH region. Moreover, the behaviour of temperature dependent modal gain as a function of photonic energy has been predicted in the inset pictures of Figs 9 and 10. In TE mode for step SCH InGaAsP/InP heterostructures, the modal gain is found at the photonic energy ~ 0.87 eV and at corresponding lasing wavelength ~ 1.40 µm; while in TM mode the modal gain is found at photonic energy ~ 0.92 eV and at corresponding[23] wavelength ~ 1.33 µm. For InGaAlAs/InP material system based nano-heterostructure, the maximum modal gain has been found to exist at photonic energies ~ 0.82 eV, 0.92 eV and corresponding lasing wavelength ~ 1.55 µm, 1.33 µm in TE and TM modes, respectively[7,21]. These differences are due to the differences in the range of anti-guiding factors.

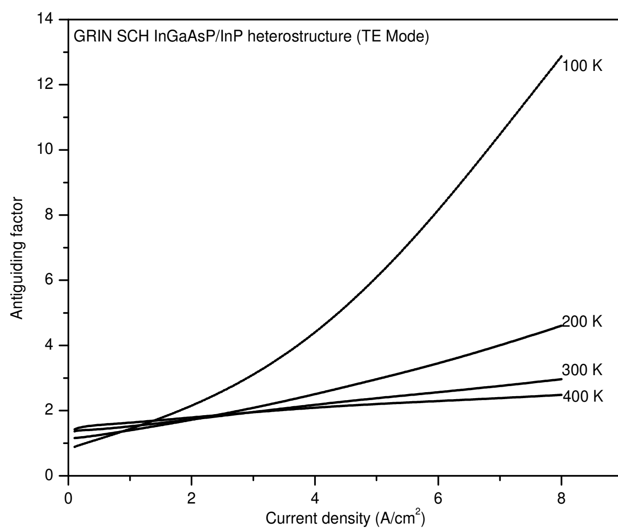

Fig. 11 — Temperature dependent anti-guiding factor for GRIN InGaAsP/InP lasing heterostructure

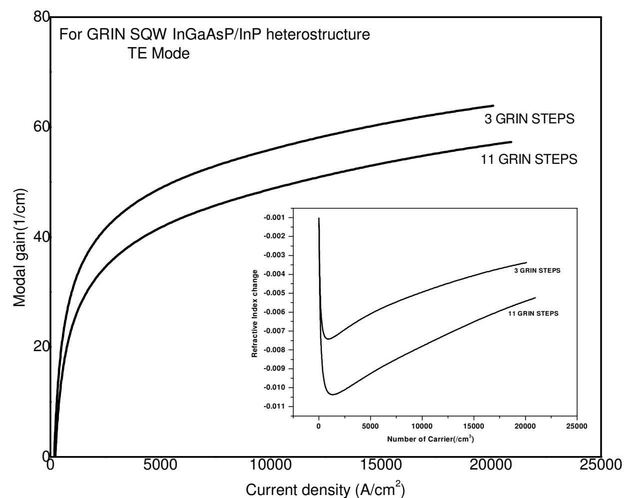

Fig. 12 — GRIN steps dependence of modal gain and refractive index change (inset figure)

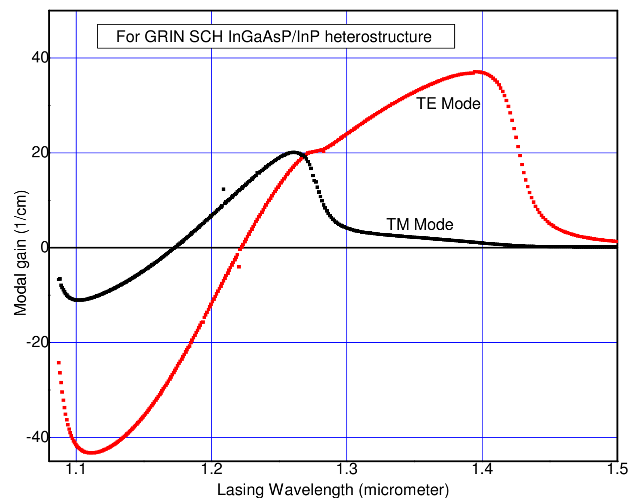

Fig. 13 — Modal gain with lasing wavelength in TE and TM modes

Experimentally, large area InGaAsP/InP double heterostructures have been grown by LPE (liquid phase epitaxy) and found to emit the radiations of wavelength[24], λ = 1.3 µm. Moreover, high-quality InGaAsP/InP heterostructures for edge-emitting 1.3 µm LED's have been prepared[25].

The temperature dependent behaviour of anti-guiding factor for the GRIN InGaAsP/InP nano-heterostructure as shown in Fig. 11, has also supported the nature of modal gain reduction with temperature. The range of anti-guiding factor is found to decrease with increasing temperature. For GRIN InGaAsP/InP material system based nano-heterostructure consisting of SQW, the highest range of anti-guiding factor (from 1 to 13) is found at 100 K, while at room temperature, this range is found to vary between 0.6 and 2, as shown in Fig. 11. A very small value is highly desirable for lasing applications because the large values can produce anti-guiding and beam filamentation. Moreover, the decreasing rate of modal gain with temperature is high with in TE mode rather than TM mode. Obviously, for a lasing nano-heterostructure, the anti-guiding factor is the responsible quantity for the material gain to exist in the heterostructure.

The GRIN steps (layers) dependence of modal gain as a function of current density for SQW based InGaAsP/InP nano-heterostructure at 300 K is shown in Fig. 12. Behaviour of carrier concentration dependent refractive index change for different GRIN steps of the structure is shown in Fig. 13. In Fig. 12, the downward shifting in the modal gain can be seen with increase in number of GRIN steps due to the reducing of the number of electrons in the optical cavity. In the inset picture of Fig. 12, the proportional behaviour of modal gain and refractive index change for same number of GRIN steps in the heterostructure is predicted. Fig. 13 shows the modal gain with lasing wavelength for GRIN InGaAsP/InP nano-heterostructureThe structure provides maximum gain at the wavelength of 1.40 µm (within TE mode) and 1.25 µm (within TM mode); hence such nano-heterostructures are very useful as a source of wavelengths in the NIR (near infra-red) region (Fig.13).

4 Conclusions

The modal gain characteristics along with optical losses have been investigated theoretically within TE and TM polarization modes for GRIN-$In_{0.90}Ga_{0.10}As_{0.59}P_{0.41}$/InP lasing nano-heterostructure taking into account number of quantum wells as active layers inserted between barriers. In addition, the behaviour of saturated modal gain, transparency current density and maximum optical loss for the single and MQWs (multiple quantum wells) based nano-heterostructures have also been studied. Moreover, temperature and GRIN dependence of modal gain characteristics with in TE and TM mode have been studied. Under simulation, the anti-guiding factors (a substantial parameter for optical gain) along with modal gain as a function of photonic energy and lasing wavelength at different temperatures have also been investigated. The maximum gain is achieved in the NIR (near infra-red) region at the wavelength ~1.40 µm and ~1.25 µm in TE and TM polarization modes, respectively, hence such nano-heterostructures are very useful as a source of wavelengths in the NIR (near infra-red) region.

Acknowledgement

The work presented was supported by University Grants Commission (UGC) Ref. F. No. 42-1067/2013 (SR), Government of India, New-Delhi. Authors are also thankful to Dr Tso-min Chou, Department of Electrical Engineering, Southern Methodist University, Dallas, TX, USA for his technical support.

References

1 Alvi P A, Gupta Sapna, Siddiqui M J, Sharma G & Dalela S, *Physica B Condensed Matt,* 405 (2010) 2431.
2 Alvi P A, Gupta Sapna, Vijay P, Sharma G & Siddiqui M J, *Physica B Condensed Matt,* 405 (2010) 3624.
3 Hirayama H, Miyake Y & Asada M, *IEEE J Quantum Electron*, 28 (1992) 68.
4 Feldmann J, Peter G, E Göbel O, Leo K, Poland H-J, Ploog K, Fujiwara K & Nakayama T, *Appl Phys Lett* 51 (1987) 226.
5 Morin S, Deveaud B, Clerot F, Fujiwara K & Mitsunaga K, *IEEE J Quantum Electron*, 28 (1991) 1669.
6 Hersee S D, Cremoux B de & Duchemin J P , *Appl Phys Lett*, 44 (1984) 476.
7 Alvi P A, Lal Pyare, Dalela S & Siddiqui M J, *Physica Scripta*, 85 (2012) 035402.
8 Yang Wang, Ying-Ping Qiu, Jiao-Qing PAN, Ling-juan Zhao, Hong-Liang Zhu & Wei Wang, *Chin Phys Lett*, 27 (2010) 114201.
9 Bugajski M, Mroziewicz B, Reginski K, Muszalski J, Kubica J, Zbroszczyk M, Sajewicz P, Piwonski T, Jachymek A, Rutkowski R, Ochalski T, Wojcik A, Kowalczyk E, Malag A, Kozlowska A, Dobrzanski L & Jagoda A, *Opto-Electronics Rev,* 9 (1) (2001).
10 Sapkota Durga Prasad, Kayastha Madhu Sudan & Wakita Kiochi, *Opt Quant Electron*, 45 (2013) 35.
11 Rohr Carsten, Abbott Paul, Ballard Ian, Connolly James P & Barnham Keith W J, Mazzer Massimo, Button Chris, Nasi Lucia, Hill Geoff & Roberts John S, Clarke Graham & Ginige Ravin, *J of Appl Phys*, 100 (2006) 114510.
12 Alvi P A, Gupta Sapna, Sharma Meha, Jha Swati & Rahman F, *Physica E Low Dimension Systems & Nanostructures*, 44 (2011) 49.
13 Gupta Sapna, Rahman F, Siddiqui M J & Alvi P A, *Physica B Condensed Matt,* 411 (2013) 40.
14 Wu Ya-Fen, *Indian J Pure & Appl Phys,* 51 (2013) 39.
15 Lenka T R & Panda A K, *Indian J Pure & Appl Phys,* 49 (2011) 416.
16 Lal Pyare, Dixit Shobhna, Dalela S, Rahman F & Alvi P A, *Physica E Low Dimension Systems & Nanostructures*, 46 (2012) 224.
17 Pandey S K, Ramrakhiani M & Chandra B P, *Indian J Pure & Appl Phys,* 41 (2003) 719.
18 Zhang Wendong, Xue Chenyang , Xiong Jijun, Xie Bin, Wei Tianjie & Chen Yong, *Indian J Pure & Appl Phys,* 45 (2007) 294.
19 Selmic Sandra R, Chou Tso-Min, Sih Jiehping, Kirk Jay B, Mantie Art, Butler Jerome K & Evans Gary A, *IEEE J On Selected Topics in Quantum Electronics*, 7 (2001) 340.
20 Chinn S R, Zory P S & Reisinger A R, *IEEE J Quantum Electron,* 24 (1988) 2191.
21 Alvi P A, Lal Pyare, Yadav Rashmi, Dixit Shobhna & Dalela S, *Superlattices & Microstructures*, 61 (2013) 1.
22 Chuang S L, *Phys of optoelectronics dev,* Wiley, New York (1995).
23 Yadav Rashmi, Lal Pyare, Rahman F, Dalela S & Alvi P A, *Int J of Modern Phys B,* 28 (2014) 1450068.
24 Volkov V V, Luyten W, Landuyt J Van, Férauge C, Oksenoid K G, Gijbels R, Vasilev M G, Shelyakin A A & Lazarev V B, *Physica Status Solidi (a),* 140 (1993) 73.
25 Novotný J, Vyhnalík L & Zelinka J, *Crystal Res & Tech,* 28 (1993) 19.